Orientation of 4-n-octyl-4'-cyanobiphenyl molecules on graphene oxide surface via electron–phonon interaction and its applications in nonlinear electronics

Dharmendra Pratap Singh, Yaochen Lin, Jean-François Blach, Hamadi Khemakhem, Christian Legrand, Redouane Douali, Benoit Duponchel

Cite this: DOI: 10.1039/xxxxxxxxxx

Orientation of 4-n-octyl-4'-cyanobiphenyl molecules on graphene oxide surface via electron-phonon interaction and its application in nonlinear electronics†

Dharmendra Pratap Singh,*[ab] Benoit Duponchel,[b] Yaochen Lin,[a] Jean-François Blach,[c] Hamadi Khemakhem,[d] Christian Legrand,[a] and Redouane Douali[a]

Received Date
Accepted Date

DOI: 10.1039/xxxxxxxxxx

www.rsc.org/journalname

We investigate the graphene oxide (GO) dispersed 4-n-octyl-4'-cyanobiphenyl (8CB) hybrid system in order to reveal the long range molecular interactions. Polarized optical microscopy envisages the vertical orientation of 8CB molecules on the GO surface. The bulk orientation of the 8CB molecules significantly depends upon the concentration of GO. The mechanism of so obtained vertical orientation was further investigated by using Raman and Fourier transformed infrared spectroscopy. We have found that the electron−phonon interaction, between the cyano (CN) functional group of 4-n-octyl-4'-cyanobiphenyl and phonons of GO, is responsible for the vertical orientation of the 8CB molecules over the GO surface. The role of CN functional group, orientational order parameter and defect intensities have been quantitatively analyzed to support the observations. We have also explored the possibility of integrating the nonlinear electronic applications of the hybrid system by studying the current−voltage (I−V) characteristics. The I−V curves of hybrid system have shown the 10^3 order higher current in comparison to pristine 8CB material which is due to the combined effect of enhanced charge carrier mobility and the formation of GO networking.

1 Introduction

The complex processing of graphene has led to the development of graphene oxide (GO) which is easily soluble in aqueous media and can be simply processed over the large area of substrate with cost-effectiveness. This advantage makes GO suitable for the various groundbreaking applications like guided electro−optical switching[1], surface mountable long life supercapacitor[2], blue photoluminescence[3], tunable sieving of ions using graphene oxide membranes[4], and many more. During the conversion process from graphene to GO, the electronic properties are compromised depending upon the degree of oxidation; therefore, the controlled oxidation for the electronic purpose is a mandatory parameter to keep in mind. Various methods have been proposed to enhance the electronic properties of GO like thermally driven phase transformation method[5] and by varying the sp^2 fraction of carbon.[6] In the recent years, development of 2D material−liquid crystals by two different methods has been suggested in which the dispersion of 2D materials in a liquid crystalline host and the liquid crystal phase arising from dispersions of 2D materials in organic solvents are considered that leads to the modern opto−electronic and display applications of such systems.[7] GO−liquid crystals and GO dispersed liquid crystals have been extensively studied for the industrial applications as well as for the fundamental aspects during the last few years.[8–16] It is well-known fact that liquid crystalline materials are composed of a central phenyl core attached with a flexible aliphatic tail whereas graphene/GO is also made of carbon atoms arranged in a hexagonal lattice. This structural similarity between liquid crystals and graphene/GO is fundamentally responsible for the coupling in these materials via π-π interactions. Recently, a variety of investigations have been carried out for the GO dispersed−LC matrix in which various applications are revealed,[12–21] among those the hybrid graphene-nematic LC light scattering device, formation of lyotropic nematic phase and faster electro-optical switching are interesting findings. The use of alignment layer is an essential procedure to provide a particular orientation to LC molecules on the ITO surface in order to make any device. Based on the influence of alignment layer and sur-

[a]*Unité de Dynamique et Structure des Matériaux Moléculaires (UDSMM), Université du Littoral Côte d'Opale, 62228 Calais, France. Fax: 03 21 46 36 42; Tel: 03 21 46 57 81; E-mail: Dharmendra.singh@univ-littoral.fr*
[b]*Unité de Dynamique et Structure des Matériaux Moléculaires (UDSMM), Université du Littoral Côte d'Opale, 59140 Dunkerque, France*
[c]*Université Artois, CNRS, Centrale Lille, ENSCL, Université Lille, UMR 8181, Unité de Catalyse et Chimie du Solide (UCCS), F-62300 Lens, France*
[d]*Laboratoire des Matériaux Multifonctionnels et Applications, Faculté des sciences de Sfax, Université de Sfax, Tunisie.*
† Electronic Supplementary Information (ESI) available: [details of any supplementary information available should be included here]. See DOI: 10.1039/b000000x/

face anchoring, LC molecules orient parallel or perpendicular to the substrate. Although, few efforts have already been made to disclose the influence of graphene and GO on the alignment of LC molecules, but the complete mechanism of the orientational coupling is still not clear.[22] Malik *et al.*[23]. have used the dispersion of a small concentration of GO in an electroclinic LC and reported the vertical alignment of molecules whereas planar alignment of ferroelectric LC molecules on the multilayer graphene coated ITO has been demonstrated by Singh *et al.*[24]. In addition to this, a simulation study of Density Functional Theory (DFT) is reported for the preferred orientation of 8CB LC molecules on the lithium niobate Z−cut surface by Braun *et al.*[25] in which they demonstrated that 0001 or $000\bar{1}$ surface of lithium niobate bounds with the C≡N group of 8CB liquid crystal. They also stated that the interface energy and vertical configuration strongly depend on the surface polarization. Recently, Singh *et al.*[26] have reported the synthesis of 3D vertically aligned few−layered graphene nanoflakes by using chemical vapour deposition. In this study, authors have shown that vertically aligned structures, assisted with partially reduced graphene oxide, can form interconnected micro voids which facilitate the ionic and electronic transport pathway where residual functional groups of partially reduced graphene oxide play an important role. The observations presented in ref. 25 and 26 provide new track to investigate the orientational interactions between the LC molecules and the GO flakes in accordance with the role of functional groups. Most recently, Uchida *et al*[27]. have shown that if cyano (CN) group is present at the terminal position of a LC compound, it causes specific negative magneto−LC effects. They have verified this effect on the basis of racemic magnetic dipolar interactions. With a similar approach, we investigate the possible interaction of CN with the surface of GO flakes and its effect on the orientation of 8CB molecules via electron−phonon interaction. Nonlinear electronic applications of organic hybrid systems have attracted the immense interest of scientific community.[28] The term "nonlinear electronics" is analogous to the fact when current doesn't follow a linear relation with the applied voltage. This fundamental fact originates the current and/or voltage regulated devices. Due to easy current/voltage regulation, the nonlinear electronics is preferred over the ohmic circuits where current linearly depends on the applied voltage. At present, the organic molecules, rich in charge carriers, are utilized as organic light emitting diodes (OLEDs), photo-detectors, organic field effect transistors (OFETs), detectors etc. In this study, we have also examined the nonlinear electronic applications of 8CB+GO hybrid system.

In the present article, 8CB liquid crystal−GO hybrid material has been prepared with the variation of GO content in 8CB anisotropic medium and interactions of LC molecules with that of GO surface are analyzed by the polarized optical microscopy, Raman and Fourier-transform infrared spectroscopy. Electron-phonon interactions are believed to take place between the electrons present on C≡N group with the phonons of GO which leads to the vertical alignment of LC molecules on the surface of GO. The role of point−like defects and disordering in the GO are also quantified to understand the nature of orientation of LC molecules on the GO surface.

2 Experimental details

2.1 Materials

The 4-n-octyl-4'-cyanobiphenyl (8CB) liquid crystalline (LC) material was purchased from Merck and used without any further purification. The molecular structure of 8CB is shown in Fig. 1(a). The mesophase sequence for 8CB is Crystal (Cr) − smectic A (SmA) − nematic (N) − isotropic (Iso). The SmA−N and N−Iso phase transitions, upon slow heating of 2 ^{o}C/min, occurred at 33.86 (306.86 K) and 40.80 ^{o}C (313.8 K) respectively. GO was synthesized from commercially available graphite (Alfa aesar, 99.999 %) following the standard Hummers method. The detailed synthesis and characterizations of GO have already been reported by us.[16] The lateral size distribution of GO flakes was recorded by the high resolution scanning electron microscope (SEM) and depicted in Fig. 1(b). The observed size distribution of GO flakes was found to be in the range of 10−40 nm. The histogram of lateral size distribution of GO flakes is presented as an inset of Fig.1 (b).

2.2 Preparation of hybrid material

0.5 mg/ml suspension of GO was first prepared in toluene. Toluene was chosen as solvent because of its low dipole moment of 0.36 D and provides impressive homogenous GO suspension, stable for a long duration. The solvents like Tetrahydrofuran (THF) or Dimethylformamide (DMF) show comparatively larger dipole moments of 1.75 and 3.82 D respectively. Their polar nature may produce some polarity effects if they remain as residue in the hybrid system. The suspension was subjected to ultrasonication for 2 hr followed by the magnetic mixing by using a magnetic stirrer for next 2 hr. After analyzing the stability of this suspension for a period of one week, it was added to liquid crystal by maintaining the weight ratio (wt/wt %) of GO to be 0.02, 0.2, and 0.4 in 8CB LC. The aforementioned mixing processes (ultrasonication and magnetic mixing) were repeated to ensure the homogenous mixing of GO and LC material. Toluene was then carefully evaporated from the hybrid mixtures. The evaporation time was fixed for more than 24 hr in order to remove the solvent completely.

2.3 Characterization methods

Polarized optical micrographs (POMs) were recorded by Zeiss AXIO attached with Infinity-2 software at 10X optical magnification. For POM observations, pure 8CB and 8CB+GO hybrid materials were filled in 50 μm thick sample cells (AWAT, Poland). The thick sample cells were used to avoid the screening of large scale GO flakes at the opening of capillary in sample cells. The temperature during these measurements was controlled by using a Linkam THMS 600 heating/cooling stage with an accuracy of $\pm$ 0.1 ^{o}C. All the sample cells were sealed by UV glue (Norland, NOA68) to avoid the leakage of material from sample cells at high temperature. Raman spectroscopic measurements were recorded in backscattering configuration using a Horiba Labram HR Spectrometer. The spectrometer had a wave number resolution better than 1 cm^{-1} and was equipped with a microscope (Olympus BX41), with the laser diode of 784 nm emission lines at a power of 4 mW and

with a CDD detector. The room temperature (298K) FTIR measurements were carried out on Nicolet iS5 (Thermo Scientific) by using ATR arrangement. Nonlinear current−voltage (I−V) characteristics of 8CB and 8CB+GO hybrid materials as a function of voltage at different temperatures were carried out using Keysight B2902A Precision Source/Measure Unit (SMU). During the I−V measurements, temperature of ITO sample cells was maintained with an accuracy of $\pm$ 0.1 ^{o}C using the Linkam TMS 93 hot plate. All the experiments were repeated several times to confirm the results.

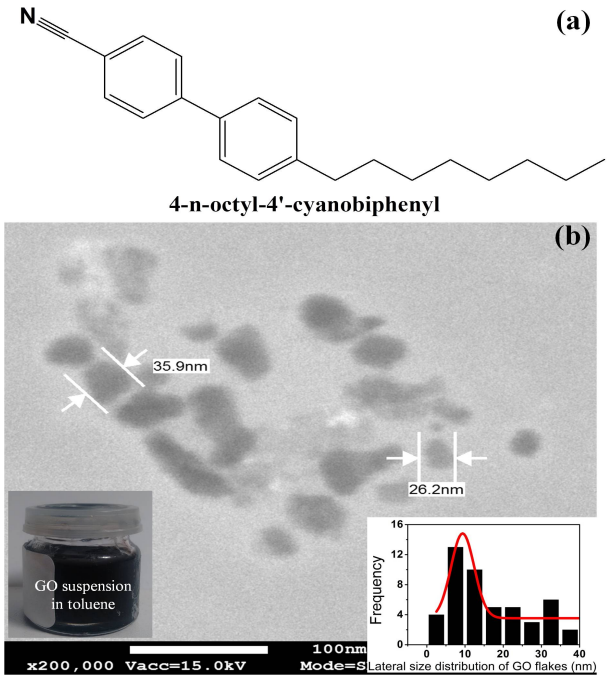

Fig. 1 (a) Molecular structure of 4-n-octyl-4'-cyanobiphenyl (8CB) liquid crystal and (b) high resolution scanning electron microscopic (SEM) image of graphene oxide (GO) flakes. Insets of fig. 1b represent the histogram of lateral size distribution of GO flakes and stable suspension of GO in toluene after one week, respectively.

3 Results and discussion

Polarized optical microscopy was performed to disclose the long range molecular interaction of 8CB molecules with that of the GO and to probe the change in the orientation of bulk LC influenced by the presence of GO flakes. Polarized optical micrographs (POMs) of pure 8CB and 8CB+GO hybrids are shown in Fig. 2. In micrographs, some black regions are appeared in the presence of GO flakes; the size of these regions increases with the increasing concentration of GO . These observations clearly show that GO significantly modifies the local orientation of LC molecules from planar to homeotropic depending on the concentration of GO. In the absence of GO, LC molecules are perfectly aligned parallel to substrate as shown in Fig. 2a, but after the dispersion of GO, the orientation of LC molecules changes successively. For the 0.02 wt% concentration of GO, the planar alignment of LC molecules remains predominant whereas molecules align principally perpendicular to substrate (homeotropic configuration) when the concentration of GO reaches to 0.4 wt%. For the intermediate dispersion concentration of GO, the orientation of LC molecules represents a merged state of the planar and homeotropic orientations. It should be keep in mind that the local homeotropic alignment of molecules evidenced by POMs for the low concentration of GO can not be easily generalized in the bulk because the dispersed GO flakes probably remain at the ITO/LC interface (as proposed in paradigm, supplementary Fig. S1†, POM-c). For higher concentration, the LC molecular orientation observed in POMs, represents the bulk orientation of the hybrid material in a 50 μm $\times$ 25 mm^2 (thickness $\times$ active area of cells) confined volume. We deduced that LC molecules always vertically orient on the GO surface. This orientation is due to the interaction between polar C≡N functional group of 8CB molecules with the GO surface via electron−phonon interaction as evidenced by the Raman measurement which is discussed in the later part. The random distribution of GO in 8CB anisotropic medium leads to the bulk orientation which has been observed in POMs. The recorded POM for 0.2wt% GO dispersed 8CB (Fig. 2c) in which GO flakes migrate closer to ITO/LC interface due to viscous drift, is alike to liquid crystalline e−ink of GO dispersed−water system as reported by He *el al.*[8] For higher GO concentration, the bulk homeotropic alignment for LC molecules is observed though some illuminated regions are also visible. These regions are originated due to the scattering of light through the functional groups attached on the edges of GO flakes and not analogous to the local planar orientation of the 8CB molecules. Indeed, when local homeotropic orientation becomes predominant, the planar oriented regions should follow the predominant anchoring in accordance with minimum free energy of the stable phase. Some aspects of the homeotropic anchoring of LCs and the orientation of GO in various media have been recently presented by Hogan *et al.*[7] The real mechanism for the homeotropic orientation of LC molecules in the presence of GO and its stability with and without surfactant is still under debate. The influence of dopant on the LC orientation and possible interactions between the dopant and ITO have been studied by Yang *et al.*[29] In this article, they stated that the dopant size up to 500 nm in smectic LC stands within a weak−anchoring regime; therefore the investigated 8CB+GO hybrid material, having GO flakes size of order 10−40 nm, should also resides in a weak anchoring regime. Following this remark, no significant change should be induced in the LC orientation due to GO/ITO anchoring. Supplementary Figures† S1(i) and S1(ii) represent the paradigm for the change in 8CB LC molecular orientation in the presence of different concentration of GO and the long range GO network that leads to the bulk orientation of 8CB molecules, respectively.

Recently, Permatasari *et al.*[30] have reported the role of CN configuration on the photoluminescence of graphene quantum dots (GQDs). The PL property remarkably depends on the molecular ordering and degree of orientation of the system. They have shown that the enhanced PL was attributed to delocalized π electrons from pyridinic/C−N configuration of the GQDs. In our case, we have also expected that C≡N functional group of 8CB liquid crystal can configure new interactions with that of the C atoms present on the GO surface inducing a change in the molecular orientation as described in POMs. To confirm our hypothesis, we performed complementary characterizations as discussed below.

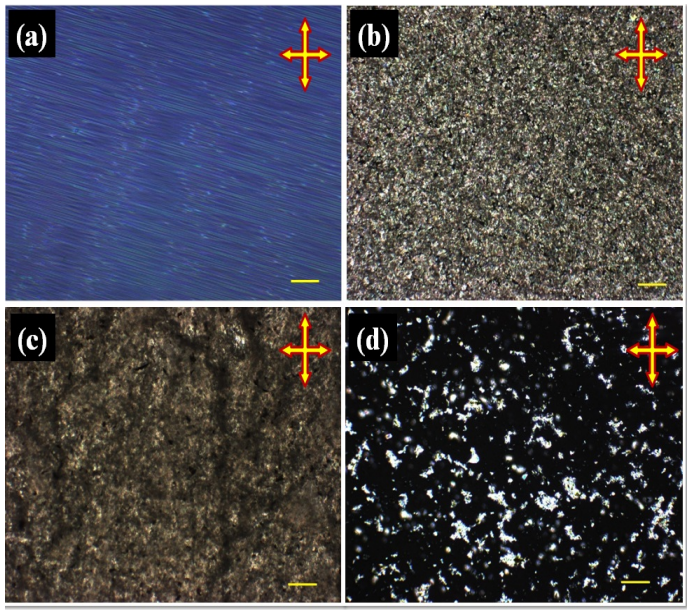

Fig. 2 Polarized optical micrographs (POMs) of (a) pure 8CB, (b) 0.02, (c) 0.2 and (d) 0.4 wt % GO dispersed 8CB hybrid material at room temperature with 10X optical resolution. The crossed arrows represent the crossed polarizer−analyzer condition. All scale bars show a distance of 10 μm. The cell thickness was 50 μm for all POMs.

Raman spectroscopy has been extensively employed to study the nCB (n= 4 to 8) liquid crystalline materials for understanding the bond−specific interactions within the material[31] and also in the colloidal and composite systems.[32,33] This technique provides in−depth information about the phase transition and order parameter of LCs based on the polarization dependence of scattering. In the present work, Raman spectroscopy was first performed to substantiate the presence of GO in LC medium. The Raman spectra of 8CB and 8CB+GO hybrid material having low (wt% $\leq$ 0.2) and high (wt% $>$ 0.2) concentration of GO at 298K (SmA phase) and 308 K (N phase) are depicted in Fig. 3a, 3b and 3c. For a given liquid crystalline phase, the Raman spectra have been found to be almost temperature independent excluding the change in the intensity of peaks. It is well known that the intra-molecular vibrations, specifically stretching modes, take place at 1100−3200 cm^{-1}.[31] The neat 8CB LC material consists of four intense peaks at 1183, 1286, 1606 and 2228 cm^{-1} corresponding to C−H deformation in the phenyl core, C−C stretching of the biphenyl ring, aromatic C−C symmetric stretching and C≡N stretching.[31]

Two low intensity peaks are also observed in the SmA phase (298K) at 1437 and 1525 cm^{-1}; these two peaks are attributed to δCH_2 and aromatic asymmetric C−C stretching, respectively.[31] In the case of neat 8CB (Fig. 3a), the intensity of these additional peaks at 1437 and 1525 cm^{-1} is lowered in the nematic phase (308K) with respect to the SmA phase (298K). If the LC molecules are not well aligned in the SmA phase, smectic layers cause scattering due to their positional order whereas in the nematic phase, LC molecules have only orientational order that gives rise to lower scattering. For 8CB+GO hybrid material having low GO concentration, it is important to notice that the Raman peak associated to δCH_2 located at 1437 cm^{-1} is feebly suppressed (Fig. 3b) whereas

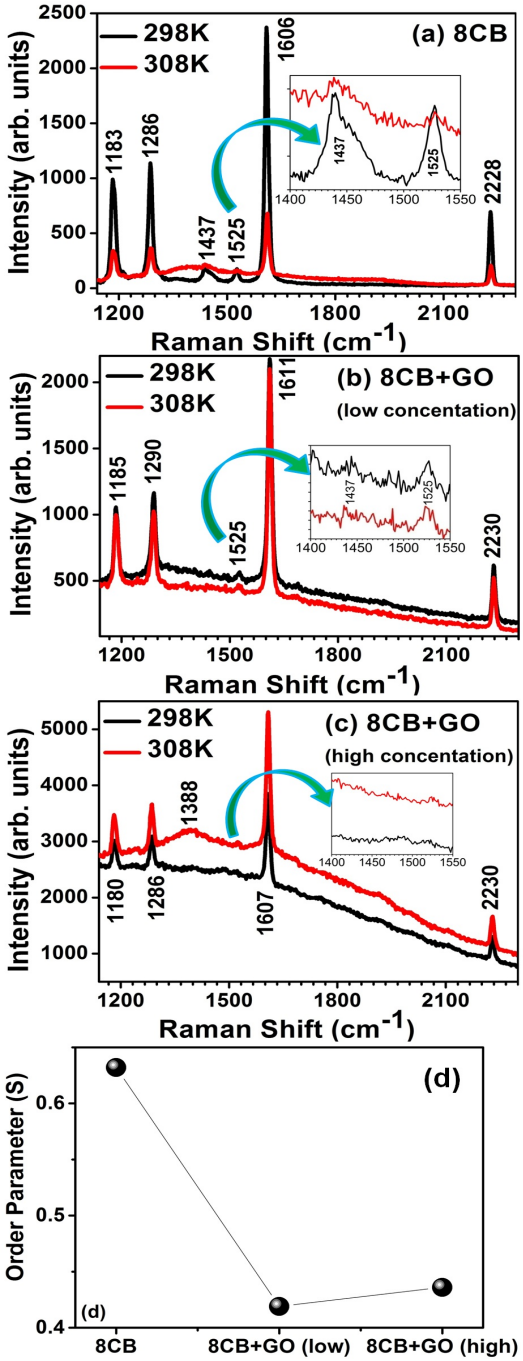

Fig. 3 Experimental Raman spectra of (a) 4-n-octyl-4'-cyanobiphenyl (8CB), (b) 8CB+graphene oxide (GO) hybrid material for low concentration of GO (wt % $\leq$ 0.2), (c) 8CB + GO hybrid material for high concentration of GO (wt % $>$ 0.2), whereas (d) represents the orientational order parameter for 8CB and 8CB+GO hybrid material. The Temperature 298 K represents the smectic A (SmA) phase whereas 308 K shows the nematic (N) phase of 8CB material. Insets of Fig. (a), (b) and (c) represent the enlarged area of Raman spectra for the regime of 1400−1550 cm^{-1}.

in the case of 8CB+GO hybrid material, having high GO concentration (Fig. 3c), both δCH_2 and aromatic asymmetric C−C stretching peaks are not visible. This phenomenon suggests that the presence of GO significantly modifies the band dynamics of 8CB. The presence of GO in the anisotropic medium of 8CB has been confirmed by the Raman spectroscopy. For lower concentration of GO (wt% $\leq$ 0.2),the Raman spectrum of 8CB+GO hybrid material exhibits almost similar vibration bands in comparison to that of the pure 8CB whereas an induced Raman peak, attributing to D band of carbon based material, at 1388 cm^{-1} has been observed for high concentration of GO (wt% > 0.2). The induced D band is an evidence of the $\pi-\pi$ interactions between the carbon atoms of 8CB liquid crystal and GO.[34] The existence of low concentration of GO in 8CB was further confirmed by the FTIR which is discussed in the later part of manuscript. In the 8CB material, the peak associated to C−H deformation in phenyl core was observed at $\approx$ 1183 cm^{-1} which has been shifted at 1185 cm^{-1} (for GO wt % $\leq$ 0.2, Fig. 3b) and 1180 cm^{-1} (for GO wt % > 0.2, Fig. 3c) in the 8CB+GO hybrid material, that is the consequence of the formation of hybrid material. Gleeson *et al.*[31] have utilized the aromatic C−C symmetric stretching Raman band positioned at $\approx$ 1606 cm^{-1} to estimate the orientational order parameter of nematic and twist-bend nematic LC phases as this band was found to be highly polarized along the long molecular axis of the rod-like molecules. By using the LZNS (Luckhurst, Zannoni, Nordio and Segre) theory[35], they performed the polarized Raman scattering (PRS) measurements to determine the orientational order parameter across the nematic temperature range. Yokoyama *et al.*[36] have reported a simple model−free method to estimate the orientation order parameter (S) of molecules in the amorphous OLED based on the absorption spectroscopy. In the present investigation, we have followed the Yokoyama's approach using the Raman spectroscopy with a fundamental concept of the scattering in the isotropic and nematic phases. In the isotropic phase, all molecules are randomly orientated whereas in nematic phase, the molecules acquire an orientational order. Therefore, by integrating the Raman peaks in isotropic and nematic phases, we can estimate the degree of orientational order. Using this approach, we obtained the following simple empirical relationship between the orientational order parameter (S) and the Raman peak intensity-

$$S = 1 - \frac{I_N}{I_{Iso}} \quad (1)$$

Where S is the orientational order parameter, and I_N and I_{Iso} are the Raman intensities of the C≡N band in the nematic and isotropic phases respectively. I_N and I_{Iso} have been evaluated at 308 and 328 K, respectively (Fig. S3).

The simple analysis and estimated values of orientational order parameter by accounting the CN stretching bands are in good agreement with the previously observed values for the orientation order parameter of the 8CB material.[31] The calculated values of the orientational order parameter for the 8CB and 8CB+GO hybrid material at low and high concentration of GO were found to be 0.632, 0.419 and 0.436, respectively (Fig. 3d).

We have checked the variation of intensity ratio (I_{298K}/I_{308K}) as a function of concentration for aromatic C−C symmetric stretching at $\approx$ 1600 cm^{-1} and CN stretching at $\approx$ 2200 cm^{-1} for the 8CB LC and 8CB+GO hybrid material having low (wt % $\leq$ 0.2) and high (wt % > 0.2) dispersion concentration of GO flakes as shown in Fig. 4a and 4b respectively. We have observed that the both bands (i.e. aromatic C−C symmetric stretching and CN stretching) follow similar I_{298K}/I_{308K} behavior. In addition to this, we have also checked the variation of Raman intensity for aforementioned bands at 308 K which is depicted in Fig. 4c. This curve suggests that the intensity of both Raman bands increases in the presence of GO. As aromatic C−C symmetric stretching band reveals the strongest scattering and polarization dependent nature, therefore, it can be used to determine the orientational order parameter of LC material as shown by Gleeson et al.[31] whereas CN stretching band discloses the polarity dependent interactions, therefore it can be utilized to establish the preferred alignment of LC molecules with the surface of dopant. In the present case, our target is to disclose the interaction of 8CB molecules with the surface of GO flakes with a motive to find out the role of CN functional group in the molecular orientation and existence of electron−phonon interaction in the investigated hybrid system.

To disclose the existence of electron−phonon interaction in 8CB+GO hybrid material, we recorded the Raman spectra of GO in pristine form and in the presence of 8CB anisotropic medium having wt % > 0.2 concentration of GO (Fig. 4d). To measure the Raman spectrum of GO in 8CB medium, a narrow laser beam was precisely focused with the help of microscope at the position where GO flakes were clearly visible and Raman spectrum was recorded. The Raman spectrum of pristine GO consists of the D peak located at 1319 cm^{-1} and G peak at 1584 cm^{-1}, caused by the disorder induced breathing of sp^2 rings and the first order scattering of the E_2g phonon of sp^2 carbon atoms, respectively.[37] D band is commonly observed in all sp^2 carbon lattices attributing to the stretching of C−C bond and its intensity provides the information about the size of in−plane sp^2 domains. In addition to this, the D band remarkably depends on the intensity of laser radiation. It up−shifts linearly with the increasing power of laser radiation. Usually, electron−phonon interactions are explored through chemical doping, in which the charge carrier density is modified by introducing an appropriate amount of the impurities. In the low dimensional systems, electric field effect is an alternative method for changing the charge carrier density.[38,39] On the other hand, the shift in G band frequency is a consequence of electron−phonon interactions in any hybrid system. In the investigated anisotropic medium, a shift of 24 cm^{-1} in G band was observed for GO, (Fig. 4d), which is evident to the electron−phonon interactions between the phonons of GO and lone−pair electrons present on the C≡N functional group of 8CB material. In Raman spectra, the ratio of D and G band peak intensities is used to characterize the degree of disorder. The D mode is dispersive whereas the G peak is not dispersive. The intensity of G peak is analogous to the presence of six−fold aromatic rings. Traditionally, the I_D/I_G intensity ratio is inversely proportional to the average size of the sp^2 domains for low defect densities but this relation fails if defect density is high.[37] In our case, we considered small defect densities. The I_D/I_G is deduced for the GO in pristine form and in anisotropic medium and has been obtained to be 1.22 and 1.02 respectively.

The lower I_D/I_G ratio for GO in anisotropic medium indicates the larger in−plane sp^2 domains within the limit of low defect density. I_D/I_G increases with increasing disorder in accordance to the Tuinstra and Koenig equation[40]

$$\frac{I_D}{I_G} = \frac{C(\lambda)}{L_a} \tag{2}$$

Where $C(\lambda)$ is a variable scaling coefficient and its value depends on λ, the laser wavelength. L_a is the size of sp^2 domains. The value of $C(\lambda)$ was found to be almost same for the linear regime of λ ($400 < \lambda < 800$ nm), therefore, the value of $C(\lambda) \approx 4.4$ nm is used for the investigated system.

The estimated in−plane sp^2 domains size (L_a) for GO in the absence of 8CB anisotropic medium was found to be 3.6 nm whereas it is found to be 4.31 nm in the presence of 8CB. The enhanced size of spatial sp^2 domains clearly indicates that GO comprises lesser disorder in an ordered anisotropic medium because of sp^2 sites are resonantly enhanced over sp^3 ones. This mechanism also suggests that GO flakes are self−assembled inside the 8CB medium due to higher $\pi-\pi$ interaction. The formation of self−assembly of different kinds of nano−structured materials in various liquid crystalline systems is well known and of particular interest for the opto-electronic applications.[11,41,42] Though, it is difficult to control the orientation of large size graphene and/or graphene oxide flakes inside any anisotropic medium, but few reports[43] explain the orientation control of graphene flakes by applying an external field. The dynamics of nematic LC significantly depend on the orientation of graphitic flakes,[44] but degree of orientation of flakes inside the medium is hard to determine. Unfortunately, in this investigation, the degree of orientation of the GO flakes has not been determined; nevertheless the self-assembling mechanism is concluded via the results of sp^2 domain size for the hybrid system. Ferrari *et al.*[45] have extensively studied the defect densities in graphene by varying the excitation energies Ar^+ ion doses and found that two different defect densities are possible depending on the ratio of D to G band intensity. They also mentioned the importance of taking the ratio of areas, maximum values of peak intensity and integrated intensity of peaks in the determination of defect densities. Here, we estimated the I_D/I_G ratio only by using intensities as the Raman peaks were asymmetric.

In order to confirm the existence of interactions between 8CB LC molecules and GO along with the presence of GO in 8 CB for the dispersion condition of wt % $\leq$ 0.2, we investigated the vibrational band dynamics of hybrid material by means of FTIR measurements. In the FTIR spectra of 8CB+GO hybrid materials (Fig. 5), an induced C=O stretching band analogous to pristine GO[46], has been clearly observed at 1685 cm^{-1}. The nature of C=O stretching band changes with the concentration of GO which certifies the presence of an external host (i.e. GO) into different concentrations in the 8CB medium. Aromatic C−C symmetric stretching and C≡N stretching bands were observed at $\approx$ 1600 and 2223 cm^{-1} respectively. The characteristics of C≡N stretching band were extensively examined for all the concentration of GO in order to disclose its contribution in the determination of the orientation of 8CB molecules on the surface of GO flakes.

The positions of integrated centroid of C≡N and induced C=O

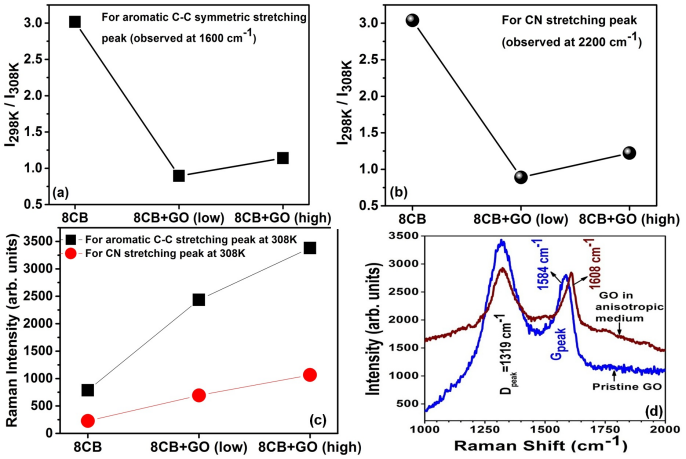

Fig. 4 The variation of intensity ratio (I_{298K}/I_{308K}) as a function of temperature for (a) aromatic C−C symmetric stretching at $\approx$ 1600 cm^{-1} and (b) CN stretching at $\approx$ 2200 cm^{-1} for 8CB LC and 8CB+GO hybrid material having low (wt % $\leq$ 0.2) and high (wt % > 0.2) dispersion concentration of GO flakes. (c) shows the change in Raman intensity of aromatic C−C stretching and CN stretching peaks at 308 K whereas (d) shows the Raman spectra of GO in pristine form and in the anisotropic (8CB) medium.

stretching bands are plotted as a function of GO concentration and shown in Fig. 6. It is clear that the addition of 0.02 wt % of GO in the 8CB LC causes a feeble up shift of C≡N stretching band. Afterward, the C≡N centroid position starts descending with increasing GO concentration. The shift in C≡N centroid position could be understood by the fact that the nitrogen lone−pair electrons have an anti−bonding character and electron donation to the GO surface may change the strength of C≡N band. This phenomenon leads to the disruption of conjugation induced by the π−coordination of C≡N functional group and GO surface. This mechanism might be the reason for the occurrence of electron−phonon interactions in 8CB+GO hybrid material. For the 0.4 wt % dispersion concentration of GO in 8CB, the POM, Raman and FTIR spectra of the hybrid material are notably different with that of the neat 8CB as well as with the other concentration of GO. Therefore, this dispersion concentration is considered to be optimized for achieving the vertical orientation of 4-n-octyl-4'-cyanobiphenyl (8CB) molecules (i.e. homeotropically aligned 8CB molecules in bulk) on the GO surface however the scattering of light from the edges of GO still needs to control. The band position of induced C=O stretching in 8CB+GO hybrid material feebly shifts to higher wavenumber side. This shift in C=O stretching band position suggests a change in the internal ordering. Therefore, the interaction of GO surface with polar functional group of 8CB molecules shows a strong correlation between the shift of C=O stretching frequency and the change in the molecular orientation of the host 8CB.

Electronic charge transport and current−voltage characteristics on the graphene oxide based systems have been extensively studied.[6,47,48] The electronic properties of carbon nanostructured material/liquid crystal composites have also attracted the attention of researchers but limited reports are available on this topic;[49] therefore, we have investigated the nonlinear electronic applications of 8CB+GO hybrid material.

Fig. 7 shows the nonlinear current−voltage (I−V) curves for

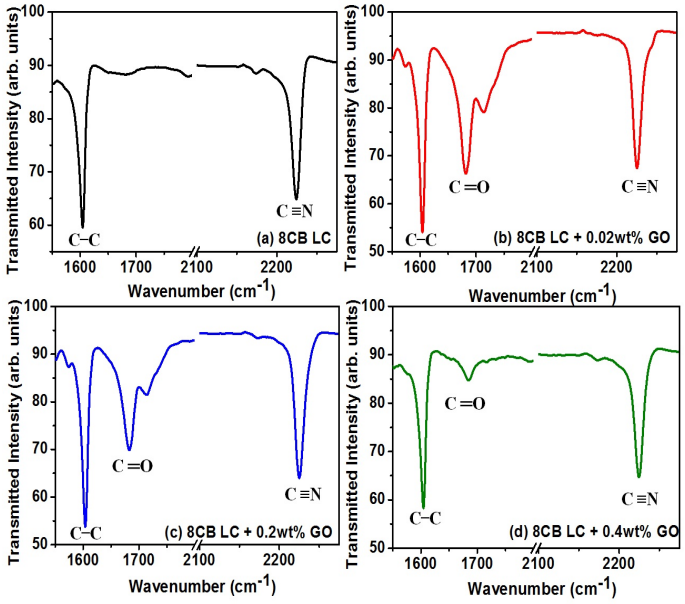

Fig. 5 Fourier-transform infrared (FTIR) curves of (a) pure 8CB, (b) 8CB + 0.02 wt % GO, (c) 8CB + 0.2 wt % GO and (d) 8CB + 0.4 wt % GO hybrid materials for the wave number interval of 1550−2275 cm^{-1} at room temperature. The scale is made to break at 1800−2100 cm^{-1} for better resolution. Complete FTIR spectra are shown in supplementary† Fig. S2.

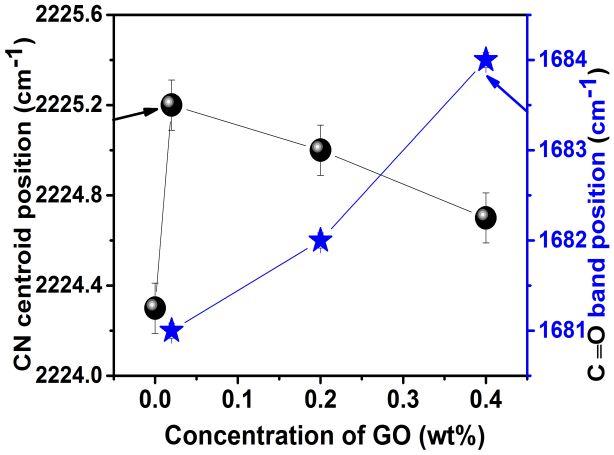

Fig. 6 C≡N band centroid and induced C=O band positions in 8CB+GO hybrid material as a function of GO concentration. The error bars represent the maximum error of ± 0.005 % in the experimental data.

the neat 8CB and 8CB+GO hybrid materials recorded at 298 and 308 K. The I−V curves of 8CB+GO hybrid system exhibit nonlinear diode like trend in the positive and negative voltage regimes. Usually in the absence of a bias field, no transport of charge carriers is expected to take place but a small magnitude of current has been observed at 0 V for the neat 8CB material and 8CB+GO hybrid system. This small current at 0 V is attributed to pseudocapacitance effect originated due to the presence of ionic charges near the electrodes (ITO). In general, pseudocapacitance effect is observed when charge carriers or ionic charges accumulate close to the electrodes and such arrangement acts as a capacitor giving rise to a small value of current at 0 V. It is well known fact that the electronic conduction remarkably depends on the molecular ordering of a system; therefore, we plotted I−V curves at two different temperatures i.e. 298 and 308 K. we have noticed that the magnitude of current at 298 K is greater than that of the 308 K which is because of higher ordering of the SmA phase as compared to the nematic phase. The nonlinearity observed in the I−V curves can be associated to the formation of a Schottky barrier as reported by Balasubramanian et al.[50]. Authors have shown that ITO/GaAs interface can form Schottky barrier that leads to the nonlinear I−V characteristics. If the I−V characteristic at Schottky barrier is thermally activated, it can be explained by the Richardson and Dushman equation[51]. In our investigation, it is evident from the POMs that GO flakes reside near the ITO and make complex interface with 8CB molecules in the dispersed state. This arrangement makes a potential barriers for the electronic charge transport. In addition, the electrons in GO are more likely to bind with oxygen due to its higher electronegativity; therefore these electrons require some energy to surmount this attractive potential barrier before making itself available for conduction. The difference in electron affinity between the carbon (C), oxygen (O) and hydrogen (H) atoms in the hybrid system would create a space charge region. The coulomb interaction between the emitted electrons and the space charge region leads to induce nonlinear I−V characteristics[47]. In our investigation, the magnitude of current in I−V curves depends on the temperature but the nonlinear nature remains the same. Phenomenologically, the relationship between I and V is governed by the following equation-[52]

$$I = A.exp\left(\frac{\beta.V^n}{k_B T}\right) \tag{3}$$

where, A is proportional constant, k_B is the Boltzmann constant, T is the temperature, β is the field lowering coefficient that depends on barrier height and n is a non-negative integer power.

To confirm the effect of space charge conduction process, we plotted log I versus $V^{1/2}$ curves, shown in figure8, for the 8CB and 8CB+0.4 wt% GO hybrid system. Linear plots are obtained at high voltage region for the both temperatures (i.e. 298 and 308 K), and the slope of the linear fit was found to be ≈ 0.5. Space charge effect is significant if the value of slope is ≥ 2. This indicates that the space charge effects are nominal and the observed I−V curves are driven by the charge carriers where temperature dependent magnitude of current is only analogous to the GO assisted molecular ordering of the liquid crystalline phase.

The observed enhancement in the magnitude of current for the GO dispersed 8CB hybrid system is particularly interesting for the nonlinear electronic applications. It is easy to fabricate large-scale nonlinear electronic devices using such hybrid systems as they are low cost material and their operating voltage is also lower as compared to the available devices in the market[53]. The micro-ampere magnitude of current is fair enough for the devices but it still needs to be improved. Such hybrid system also has high dielectric constant; therefore they can be used as high-k dielectrics in the flexible/stretchable organic electronics. Additionally, the durability of nonlinear electronic devices made of hybrid organic molecular system needs further improvements. It is important to explain the underlined mechanism for the nonlinear current enhancement.

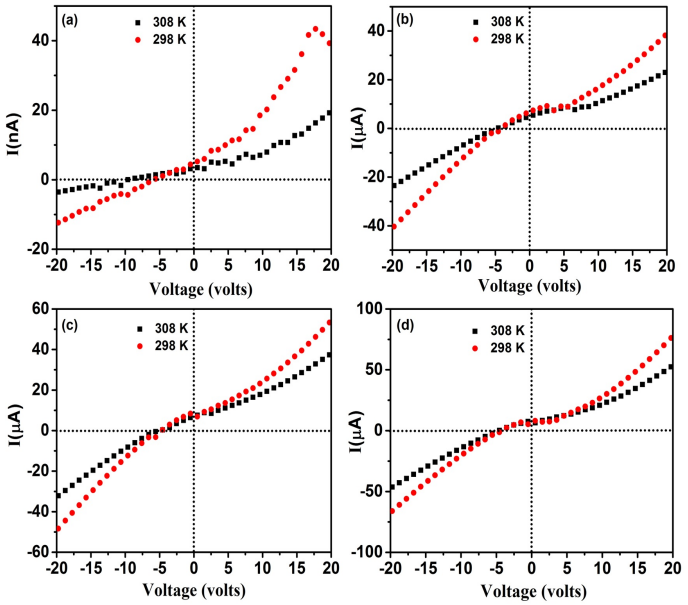

Fig. 7 Current-Voltage (I−V) curves of (a) 8CB, (b) 8CB+0.02 wt %, (c) 8CB+0.2 wt % and (d) 8CB+0.4 wt % GO dispersed hybrid systems recorded at 298 and 308 K.

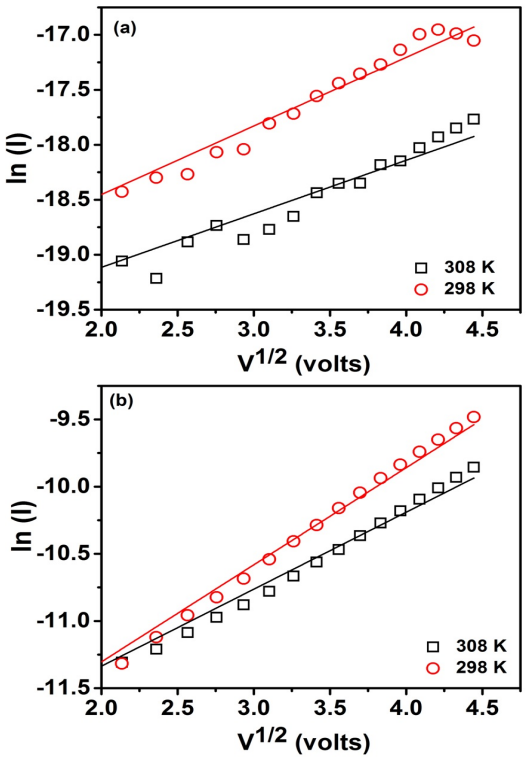

Fig. 8 Current-Voltage (I−V) characteristic curves of (a) 8CB and (b) 8CB+0.4 wt % GO dispersed hybrid systems to depict space charge effect. Solid lines represent the linear fit of experimental data.

For liquid crystalline materials, the conductivity is directly proportional to the mobility of charge carriers[54], i.e. σ=nqμ, where σ is the conductivity, n is the carrier concentration, q is the electronic charge on the carriers and μ is the mobility. The conductivity (σ) was measured by the dielectric measurement. Considering the quantity nq to be constant, the conductivity would be directly proportional to the mobility of charge carriers. In figure 9, we have shown the ratio of conductivities i.e. $\sigma_{hybrid}/\sigma_{8CB}$ to disclose the relative change in the mobility of charge carriers for the 8CB material after the dispersion of GO into different concentrations. It is clear from the figure 9 that the dispersion of GO enhances the mobility of charge carriers by the order of $\approx 10^2$. The remaining contribution might be associated to the formation of GO networking (shown in supplementary figure S1) which assists the charge carriers to transport easily in order to enhance the current in 8CB+GO hybrids by the order of 10^3.

Figure 10 depicts the variation of dielectric constant on the frequency scale for the 8CB+GO hybrid system whereas inset represents the dielectric constant versus frequency curve of the pure 8CB material at 308 K. It is observed that the dielectric constant of 8CB+GO hybrid system increases with increasing GO concentration in comparison to the pure 8CB material. The enhancement in dielectric constant is in agreement with the POM results. When the effective orientation of liquid crystalline molecules changes from planar to homeotropic, the dielectric constant increases. It is already reported in literature that the presence of carbon based material (like PCBM) increases the orientation of host system, subsequently, the dielectric constant increases.[55] According to Clausius-Mossotti-Debye equation, the dielectric constant depends on the electronic and orientation polarization and it is obvious that the observed enhancement in dielectric constant for the 8CB+GO hybrid system is due to the change in the orientation/alignment and the additional contribution from GO networking.

4 Conclusions

Herein, we have investigated the long range molecular interaction of 4-n-octyl-4'-cyanobiphenyl (8CB) molecules with that of the GO surface. Different weight percentages, ($0.02 \leq$ wt % ≤ 0.4), of the GO flakes are made to disperse in 8CB anisotropic medium and the preferred orientation of 8CB molecules on the GO surface has been investigated as a function of GO concentration. For lower GO concentrations (wt % ≤ 0.2), the bulk vertical orientation is not observed by polarized optical microscopy, whereas for the wt % > 0.2, the bulk vertical orientation has been observed. The interactions and mechanism of orientation of 8CB molecules on GO were confirmed by the complementary measurements. Raman spectroscopy confirms the formation of 8CB+GO hybrid material and the $\pi-\pi$ interactions between the 8CB molecules and GO surface. Higher GO concentration (wt % > 0.2) suppresses the asymmetric C−C stretching dynamics of the 8CB molecules. The G band frequency of pristine GO is found to shift by 24 cm^{-1} in anisotropic medium which is the consequence of electron−phonon interactions in the 8CB+GO hybrid system. Electron−phonon interactions take place between the phonons of GO and the lone pair electrons present on the C≡N functional group of 8CB material which leads the vertical orientation of 8CB molecules on the GO surface. The vertical orientation of 8CB molecules on the GO surface becomes significantly strong as the concentration of GO in 8 CB medium increases up to 0.4 wt %. The role of C≡N functional group for vertical orientation of 8CB molecules on the GO sur-

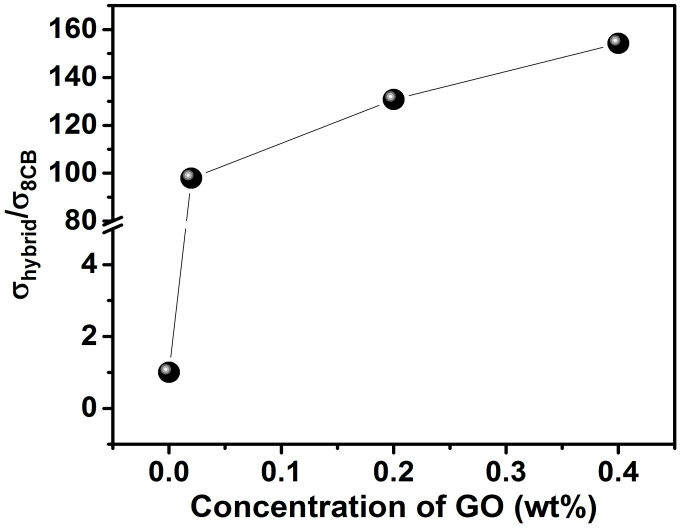

Fig. 9 Conductivity ratio, ($\sigma_{hybrid}/\sigma_{8CB}$), of 8CB+GO hybrid system with that of pristine 8CB material in order to estimate the change in charge carrier mobilities in hybrid system with respect to 8CB material. The representative ratio of conductivities was calculated at 308 K.

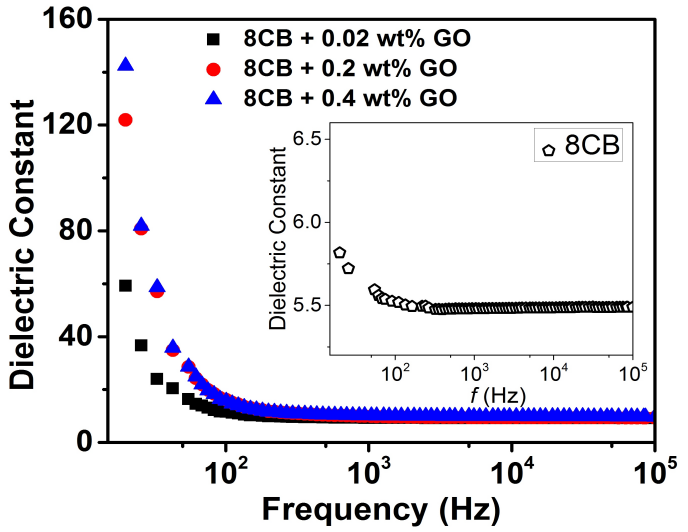

Fig. 10 Dielectric constant versus frequency curves of 8CB+GO hybrid systems at 308 K. Inset represents the dielectric constant versus frequency curve of the pure 8CB material at 308 K.

face has been verified by plotting the C≡N band centroid position versus GO concentration via FTIR measurements. By using the Tuinstra and Koenig equation and analyzing the intensity ratio of D and G band (I_D/I_G), we noticed that the spatial sp^2 domain size of GO enhances in anisotropic medium which suggests the lesser disorder in GO because of sp^2 sites are resonantly enhanced over sp^3 ones in anisotropic medium. This study reveals that the role of C≡N functional group is equally important in order to determine the interactions and preferred orientation of LC molecules with any surface in comparison to previously reported articles emphasizing over the aromatic C−C symmetric stretching band for determining the orientational order parameter of LC. The estimated order parameters by the empirical relation for the neat 8CB material and also for 8CB+GO hybrid material is found to be in good agreement with previously reported data. The presence of GO network has augmented the magnitude of current by 10^3 times in the hybrid system due to the combined effect of the fastening in the mobility of charge carriers and the formation of GO networking. It is observed that the dielectric constant of 8CB material significantly enhances after the dispersion of GO which is in agreement with the results of POMs. The investigated hybrid system has shown its potential applications in the fabrication of nonlinear electronic devices like diodes, field effect transistors and high k-dielectrics for the flexible electronics.

Supplementary Information

The spontaneous orientation of free standing GO flakes in 8 CB medium is presented by a paradigm which is shown in Fig. S1 whereas full range of FTIR spectra is shown in Fig. S2. Fig. S3 represents the Raman intensity of CN band.

Conflicts of interest

“There are no conflicts to declare”.

Acknowledgements

DPS is thankful to UDSMM, ULCO for the financial assistance. The authors sincerely thank to Prof. A. Hadj Sahraoui, the Director of UDSMM, for his continuous encouragement, support and interest in our work. We also thankfully acknowledge Mr. Paul Genevray for his help in the FTIR measurements.

Notes and references

1 R. T. M. Ahmad, T.-Z. Shen, A. R. Masud, T. K. Ekanayaka, B. Lee and J.-K. Song, *Langmuir*, 2016, **32**, 13458–13463.

2 Y. Wang, W. Lai, N. Wang, Z. Jiang, X. Wang, P. Zou, Z. Lin, H. J. Fan, F. Kang, C.-P. Wong and C. Yang, *Energy & Environmental Science*, 2017, **10**, 941–949.

3 G. Eda, Y.-Y. Lin, C. Mattevi, H. Yamaguchi, H.-A. Chen, I.-S. Chen, C.-W. Chen and M. Chhowalla, *Advanced Materials*, 2010, **22**, 505–509.

4 J. Abraham, K. S. Vasu, C. D. Williams, K. Gopinadhan, Y. Su, C. T. Cherian, J. Dix, E. Prestat, S. J. Haigh, I. V. Grigorieva, P. Carbone, A. K. Geim and R. R. Nair, *Nature Nanotechnology*, 2017, **12**, 546–550.

5 P. V. Kumar, N. M. Bardhan, S. Tongay, J. Wu, A. M. Belcher and J. C. Grossman, *Nature Chemistry*, 2014, **6**, 151–158.

6 D. Joung and S. I. Khondaker, *The Journal of Physical Chemistry C*, 2013, **117**, 26776–26782.

7 B. T. Hogan, E. Kovalska, M. F. Craciun and A. Baldycheva, *Journal of Materials Chemistry C*, 2017, **5**, 11185–11195.

8 L. He, J. Ye, M. Shuai, Z. Zhu, X. Zhou, Y. Wang, Y. Li, Z. Su, H. Zhang, Y. Chen, Z. Liu, Z. Cheng and J. Bao, *Nanoscale*, 2015, **7**, 1616–1622.

9 R. Narayan, J. E. Kim, J. Y. Kim, K. E. Lee and S. O. Kim, *Advanced Materials*, 2016, **28**, 3045–3068.

10 F. Lin, X. Tong, Y. Wang, J. Bao and Z. M. Wang, *Nanoscale Research Letters*, 2015, **10**, 435.

11 Z. Xu and C. Gao, *ACS Nano*, 2011, **5**, 2908–2915.

12 R. Basu, *Applied Physics Letters*, 2014, **105**, 112905.

13 M. Kumar and S. Kumar, *RSC Advances*, 2015, **5**, 14871–14878.

14 M. M. Qasim, A. A. Khan, A. Kostanyan, P. R. Kidambi, A. Cabrero-Vilatela, P. Braeuninger-Weimer, D. J. Gardiner, S. Hofmann and T. D. Wilkinson, *Nanoscale*, 2015, **7**, 14114–14120.

15 S. Al-Zangana, M. Iliut, G. Boran, M. Turner, A. Vijayaraghavan and I. Dierking, *Scientific Reports*, 2016, **6**, 31885.

16 D. P. Singh, V. Kumar, A. Kumar, R. Manohar, R. Pasricha, B. Duponchel, Y. Boussoualem, A. H. Sahraoui and A. Daoudi, *RSC Advances*, 2017, **7**, 12479–12485.

17 S. Al-Zangana, M. Iliut, M. Turner, A. Vijayaraghavan and I. Dierking, *Advanced Optical Materials*, 2016, **4**, 1541–1548.

18 M. Kumar, A. Gowda and S. Kumar, *Particle & Particle Systems Characterization*, 2017, **34**, 1700003/1–1700003/25.

19 S. Javadian, N. Dalir and J. Kakemam, *Liquid Crystals*, 2017, **44**, 1341–1355.

20 R. Basu, D. Kinnamon and A. Garvey, *Applied Physics Letters*, 2015, **106**, 201909.

21 V. Kumar, A. Kumar, S. Bhandari, A. M. Biradar, G. B. Reddy and R. Pasricha, *Journal of Applied Physics*, 2015, **118**, 114904.

22 R. Basu, D. Kinnamon and A. Garvey, *Liquid Crystals*, 2016, **43**, 2375–2390.

23 A. Malik, A. Choudhary, P. Silotia, A. M. Biradar, V. K. Singh and N. Kumar, *Journal of Applied Physics*, 2010, **108**, 124110.

24 D. P. Singh, S. K. Gupta, T. Vimal and R. Manohar, *Physical Review E*, 2014, **90**, 022501.

25 C. Braun, S. Sanna and W. G. Schmidt, *The Journal of Physical Chemistry C*, 2015, **119**, 9342–9346.

26 D. P. Singh, N. Soin, S. Sharma, S. Basak, S. Sachdeva, S. S. Roy, H. W. Zanderbergen, J. A. McLaughlin, M. Huijben and M. Wagemaker, *Sustainable Energy & Fuels*, 2017, **1**, 1516–1523.

27 T. Akita, D. Kiyohara, T. Yamazaki, Y. Uchida and N. Nishiyama, *Journal of Materials Chemistry C*, 2017, **5**, 12457–12465.

28 C. D. Dimitrakopoulos and P. R. L. Malenfant, *Advanced Materials*, 2002, **14**, 99–117.

29 A. Honglawan, D. S. Kim, D. A. Beller, D. K. Yoon, M. A. Gharbi, K. J. Stebe, R. D. Kamien and S. Yang, *Soft Matter*, 2015, **11**, 7367–7375.

30 F. A. Permatasari, A. H. Aimon, F. Iskandar, T. Ogi and K. Okuyama, *Scientific Reports*, 2016, **6**, 21042.

31 Z. Zhang, V. P. Panov, M. Nagaraj, R. J. Mandle, J. W. Goodby, G. R. Luckhurst, J. C. Jones and H. F. Gleeson, *Journal of Materials Chemistry C*, 2015, **3**, 10007–10016.

32 P. Lin, Q. Yan, Y. Chen, X. Li and Z. Cheng, *Chemical Engineering Journal*, 2018, **334**, 1023–1033.

33 N. Puech, M. Dennison, C. Blanc, P. van der Schoot, M. Dijkstra, R. van Roij, P. Poulin and E. Grelet, *Physical Review Letters*, 2012, **108**, 247801.

34 D. R. Dreyer, S. Park, C. W. Bielawski and R. S. Ruoff, *Chemical Society Reviews*, 2009, **39**, 228–240.

35 G. R. Luckhurst, C. Zannoni, P. L. Nordio and U. Segre, *Molecular Physics*, 1975, **30**, 1345–1358.

36 Y. Sakai, M. Shibata and D. Yokoyama, *Applied Physics Express*, 2015, **8**, 096601.

37 A. C. Ferrari and J. Robertson, *Physical Review B*, 2000, **61**, 14095–14107.

38 J. Yan, Y. Zhang, P. Kim and A. Pinczuk, *Physical Review Letters*, 2007, **98**, 166802.

39 Y. Zhu, S. Murali, W. Cai, X. Li, J. W. Suk, J. R. Potts and R. S. Ruoff, *Advanced Materials*, 2010, **22**, 3906–3924.

40 F. Tuinstra and J. L. Koenig, *The Journal of Chemical Physics*, 1970, **53**, 1126–1130.

41 A. Mertelj, D. Lisjak, M. Drofenik and M. Čopič, *Nature*, 2013, **504**, 237–241.

42 N. Behabtu, J. R. Lomeda, M. J. Green, A. L. Higginbotham, A. Sinitskii, D. V. Kosynkin, D. Tsentalovich, A. N. G. Parra-Vasquez, J. Schmidt, E. Kesselman, Y. Cohen, Y. Talmon, J. M. Tour and M. Pasquali, *Nature Nanotechnology*, 2010, **5**, 406–411.

43 F. Lin, Z. Zhu, X. Zhou, W. Qiu, C. Niu, J. Hu, K. Dahal, Y. Wang, Z. Zhao, Z. Ren, D. Litvinov, Z. Liu, Z. M. Wang and J. Bao, *Advanced Materials*, 2017, **29**, 1604453.

44 W. Tie, S. S. Bhattacharyya, Y. Gao, Z. Zheng, E. J. Shin, T. H. Kim, M. Kim, J. H. Lee and S. H. Lee, *Nanomaterials*, 2017, **7**, 250.

45 L. G. Cançado, A. Jorio, E. H. M. Ferreira, F. Stavale, C. A. Achete, R. B. Capaz, M. V. O. Moutinho, A. Lombardo, T. S. Kulmala and A. C. Ferrari, *Nano Letters*, 2011, **11**, 3190–3196.

46 D. P. Singh, B. Duponchel, Y. Boussoualem, K. Agrahari, R. Manohar, V. Kumar, R. Pasricha, G. H. Pujar, S. R. Inamdar, R. Douali and A. Daoudi, *New Journal of Chemistry*, 2018, **42**, 16682–16693.

47 I.-y. Lee, E. S. Kannan and G.-H. Kim, *Applied Physics Letters*, 2009, **95**, 263308.

48 I. B. Olenych, O. I. Aksimentyeva, L. S. Monastyrskii, Y. Y. Horbenko and M. V. Partyka, *Nanoscale Research Letters*, 2017, **12**, 272.

49 D. Volpati, M. K. Massey, D. W. Johnson, A. Kotsialos, F. Qaiser, C. Pearson, K. S. Coleman, G. Tiburzi, D. A. Zeze and M. C. Petty, *Journal of Applied Physics*, 2015, **117**, 125303.

50 N. Balasubramanian and A. Subrahmanyam, *Semiconductor Science and Technology*, 1990, **5**, 871.

51 A. L. Smith and R. Breitwieser, *Journal of Applied Physics*, 1970, **41**, 436–437.

52 M. Stuart, *British Journal of Applied Physics*, 1967, **18**, 1637.

53 D. P. Singh, Y. Boussoualem, B. Duponchel, A. H. Sahraoui, Sandeep Kumar, R. Manohar and A. Daoudi, *Journal of Physics D: Applied Physics*, 2017, **50**, 325301.

54 Y. Lin, R. Douali, F. Dubois, A. Segovia-Mera and A. Daoudi, *The European Physical Journal E*, 2015, **38**, 103.

55 J. Wu, J. Luo, N. Cernetic, K. Chen, K.-S. Chiang and A. K.-Y. Jen, *Journal of Materials Chemistry C*, 2016, **4**, 10286–10292.